Available online at www.sciencedirect.com

ScienceDirect

Procedia Structural Integrity 2 (2016) 3377–3384

Structural Integrity Procedia

www.elsevier.com/locate/procedia

21st European Conference on Fracture, ECF21, 20-24 June 2016, Catania, Italy

Transverse cracking in metal/ceramic composites with lamellar microstructure

Maria Kashtalyan[a]*, Romana Piat[b], Igor Guz[a]

[a]*Centre fo Micro- and Nanomechanics (CEMINACS), School of Engineering, University of Aberdeen, Aberdeen AB24 3UE, Scotland, UK*
[b]*Faculty of Mathematics and Natural Sciences, University of Applied Sciences Darmstadt, Germany*

Abstract

Metal/ceramic composites with lamellar microstructures are a novel class of metal-matrix composites produced by infiltration of freeze-cast or ice-templated ceramic preforms with molten aluminium alloy. The cost-effectiveness of production and relatively high ceramic content make such composites attractive to a number of potential applications in the automotive, aerospace and biomedical engineering. A hierarchical lamellar microstructure exhibited by these composites, with randomly orientated domains in which all ceramic and metallic lamellae are parallel to each other, is the result of the ice crystal formation during freeze-casting or ice templating of preforms from water-ceramic suspensions. In this paper, a single-domain sample of metal/ceramic composite with lamellar microstructure is modelled theoretically using a combination of analytical and computational means. Stress field in the sample containing multiple transverse cracks in the ceramic layer is determined using a modified 2-D shear lag approach and a finite element method. Degradation of stiffness properties of the sample due to multiple transverse cracking is also predicted.

Peer-review under responsibility of the Scientific Committee of ECF21.

Keywords: Metal-matrix composites; transverse cracking; stiffness degradation

1. Introduction

Metal/ceramic composites offer many advantages over monolithic metals and their alloys such as high specific stiffness and strength, better creep, fatigue and wear resistance, and good thermal properties. One of the new classes of metal/ceramic composites that have emerged in the recent decades are interpenetrating phase composites, in

* Corresponding author. Tel.: +44-1224-272519.
E-mail address: m.kashtalyan@abdn.ac.uk

Peer review under responsibility of the Scientific Committee of ECF21.
10.1016/j.prostr.2016.06.421

which ceramic preforms with open porosity are infiltrated with molten metal or alloy to produce composites with two three-dimensionally interpenetrating constituents (Mortensen and Llorca, 2010). Several innovative methods have been developed to produce open-pore ceramic preforms, one of which – freeze casting – is based on the physics of ice formation and involves controlled directional freezing of concentrated water-ceramic suspension (Deville, 2008). Metal/ceramic composites produced from freeze-cast alumina preforms infiltrated with aluminium-silicon alloy using a squeeze-casting technique were studied by Wanner and Roy (2008). The composites were found to possess hierarchical lamellar microstructure with randomly orientated individual regions (domains), in which all ceramic and metallic lamellae are parallel to each other. Individual domains were found to exhibit a pronounced anisotropy, with the freezing direction being the stiffest and strongest. Failure in this direction occurred in a brittle manner, while other directions were controlled by the alloy and exhibited extensive ductility (Roy, Butz and Wanner, 2010). In the subsequent studies, complete set of anisotropic elastic properties of these composites was determined experimentally using ultrasound phase spectroscopy and resonant ultrasound spectroscopy and predicted using micromechanical modelling (Ziegler et al, 2009; Ziegler et al, 2010; Roy et al, 2011). A study of single-domain samples taken from these composites was also undertaken (Sinchuk et al, 2013) focusing on the compressive response and elasto-plastic behavior. Initiation and accumulation of damage within the ceramic lamellae, mainly in the form of transverse cracking, Fig. 1, has been observed under compressive loading. Transverse cracking is also expected to occur under tensile loading due to failure strain of ceramics being less than that of metal. However, damage mechanisms in metal/ceramic composites with lamellar microstructures have not been studied in depth yet.

In this paper, a single-domain sample of metal/ceramic composite with lamellar microstructure is modeled using a combination of analytical and computational means. Stress field in the sample containing multiple transverse cracks in the ceramic layer is determined used a modified 2-D shear lag approach (Kashtalyan and Soutis, 2011; Kashtalyan and Soutis, 2013; Kashtalyan et al, 2016) and a finite element method. The Equivalent Constraint Model is then applied to predict degradation of stiffness properties of the sample due to multiple transverse cracking.

Fig. 1. Transverse cracks in ceramic layer of metal/ceramic composite with lamellar microstructure.

2. Modelling

A composite sample consisting of a ceramic layer of thickness $2h_c$ fully bonded between two metal layers of thickness h_m is considered. Ceramic layer is assumed to contain multiple tunnelling cracks, spaced uniformly with crack spacing $S = 2s$ and spanning the full thickness of the ceramic layer and depth $2w$ of the sample. The crack widening is equal to $2l$; if the crack widening is absent $l = 0$. The sample is referred to the co-ordinate system $x_1x_2x_3$, with x_1 axis parallel to the cracks (Figure 2a) and subjected to biaxial tension $\overline{\sigma}_{11}, \overline{\sigma}_{22}$ and in-plane shear loading $\overline{\sigma}_{12}$. Due to periodicity of damage and symmetry of the sample, only a quarter of the representative segment bounded by two cracks needs to be analysed (Figure 2b, c).

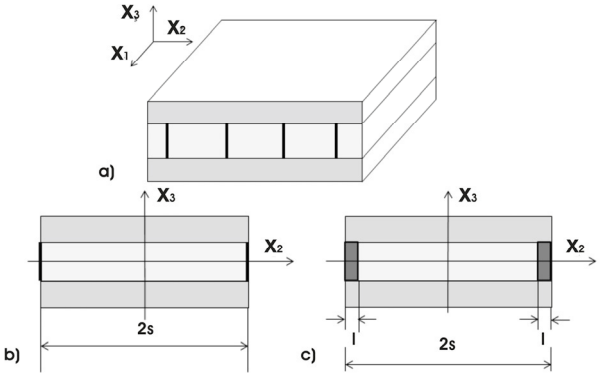

Fig. 2. (a) Schematics showing a composite sample with multiple cracks in the ceramic layer;(b) representative segment bounded by two cracks without crack widening; (c) representative segment bounded by two cracks with crack widening $2l$.

The equilibrium equations in terms of layer stresses, i.e. stresses averaged across the thickness of the layer and the depth of the sample, have the form

$$\chi\widetilde{\sigma}_{ij}^{(m)}+\widetilde{\sigma}_{ij}^{(c)}=(1+\chi)\overline{\sigma}_{ij},\quad i,j=1,2,\quad \chi=h_m/h_c \tag{1a}$$

$$\frac{d\widetilde{\sigma}_{22}^{(c)}}{dx_2}+\frac{\tau_2}{h_c}=0,\qquad \frac{d\widetilde{\sigma}_{12}^{(c)}}{dx_2}+\frac{\tau_1}{h_c}=0,\qquad \widetilde{\sigma}_{ij}^{(c)}=\frac{1}{2wh_c}\int_{-w}^{w}\int_{-h_c}^{h_c}\sigma_{ij}^{(c)}(x_1,x_2,x_3)dx_1dx_3 \tag{1b}$$

where τ_1,τ_2 are the interface shear stresses at the metal/ceramics interface. Assuming that out-of-plane shear stresses vary linearly with x_3 and in the metal layer this variation is restricted to the shear layer of thickness h_s, i.e.

$$\sigma_{j3}^{(c)}=\frac{\tau_j}{h_c}x_3,\quad |x_3|<h_c;\quad \sigma_{j3}^{(m)}=\frac{\tau_j}{h_s}(h_c+h_s-x_3),\quad h_c<|x_3|<h_c+h_s,\quad j=1,2 \tag{2}$$

the interface shear stresses τ_1,τ_2 can be expressed in terms of the in-plane displacements $\widetilde{u}_j^{(c)},\widetilde{u}_j^{(m)},j=1,2$, and shear moduli G_c,G_m of the ceramic and metal phases as

$$\tau_j=K_j(\widetilde{u}_j^{(m)}-\widetilde{u}_j^{(c)}),\quad K_j=\frac{3G_cG_m}{h_cG_m+(1+(1-\eta)/2)\eta h_mG_c},\quad \eta=h_s/h_m \tag{3}$$

The constitutive equations in terms of layer strains and stresses are

$$\begin{bmatrix}\widetilde{\varepsilon}_{11}^{(c)}\\ \widetilde{\varepsilon}_{22}^{(c)}\\ \widetilde{\gamma}_{12}^{(c)}\end{bmatrix}=\begin{bmatrix}S_{11}^{(c)} & S_{12}^{(c)} & 0\\ S_{12}^{(c)} & S_{22}^{(c)} & 0\\ 0 & 0 & S_{66}^{(c)}\end{bmatrix}\begin{bmatrix}\widetilde{\sigma}_{11}^{(c)}\\ \widetilde{\sigma}_{22}^{(c)}\\ \widetilde{\sigma}_{12}^{(c)}\end{bmatrix},\qquad \begin{bmatrix}\widetilde{\varepsilon}_{11}^{(m)}\\ \widetilde{\varepsilon}_{22}^{(m)}\\ \widetilde{\gamma}_{12}^{(m)}\end{bmatrix}=\begin{bmatrix}S_{11}^{(m)} & S_{12}^{(m)} & 0\\ S_{12}^{(m)} & S_{22}^{(m)} & 0\\ 0 & 0 & S_{66}^{(m)}\end{bmatrix}\begin{bmatrix}\widetilde{\sigma}_{11}^{(m)}\\ \widetilde{\sigma}_{22}^{(m)}\\ \widetilde{\sigma}_{12}^{(m)}\end{bmatrix} \tag{4}$$

In addition, it is also assumed that $\widetilde{\varepsilon}_{11}^{(c)}=\widetilde{\varepsilon}_{11}^{(m)}$, and crack surfaces are stress-free, i.e.

$$\widetilde{\sigma}_{22}^{(c)}\Big|_{x_2=\pm(s+l)}=0,\quad \widetilde{\sigma}_{12}^{(c)}\Big|_{x_2=\pm(s+l)}=0 \tag{5}$$

Equations (1)-(4) can be reduced to two uncoupled second-order ordinary differential equations with respect to in-plane layer stresses in the ceramic layer.

$$\frac{d^2\widetilde{\sigma}_{22}^{(c)}}{dx_2}-L_1^{(c)}\widetilde{\sigma}_{22}^{(c)}+\Omega_{11}^{(c)}\overline{\sigma}_{11}+\Omega_{22}^{(c)}\overline{\sigma}_{22}=0,\quad \frac{d^2\widetilde{\sigma}_{12}^{(c)}}{dx_2}-L_2^{(c)}\widetilde{\sigma}_{12}^{(c)}+\Omega_{12}^{(c)}\overline{\sigma}_{12}=0 \tag{6}$$

Solutions of these equations satisfying specified boundary conditions (5) are found as

$$\widetilde{\sigma}_{22}^{(c)}=\frac{1}{L_1^{(c)}}\left(1-\frac{\cosh\sqrt{L_1^{(c)}}x_2}{\cosh\sqrt{L_1^{(c)}}(s-l)}\right)(\Omega_{11}^{(c)}\overline{\sigma}_{11}+\Omega_{22}^{(c)}\overline{\sigma}_{22}),$$
$$\widetilde{\sigma}_{12}^{(c)}=\frac{1}{L_2^{(c)}}\left(1-\frac{\cosh\sqrt{L_2^{(c)}}x_2}{\cosh\sqrt{L_2^{(c)}}(s-l)}\right)\Omega_{12}^{(c)}\overline{\sigma}_{12} \tag{7a}$$

$$L_1^{(c)}=\frac{K_2}{h_m}[S_{22}^{(m)}+\chi S_{22}^{(c)}+a_1(S_{12}^{(m)}+\chi S_{12}^{(c)})],\quad L_2^{(c)}=\frac{K_1}{h_m}(S_{66}^{(m)}+\chi S_{66}^{(c)}),$$
$$\Omega_{11}^{(c)}=\frac{K_2}{h_m}(1+\chi)(S_{12}^{(m)}+a_1S_{11}^{(m)}),\quad \Omega_{22}^{(c)}=\frac{K_2}{h_m}(1+\chi)(S_{22}^{(m)}+a_1S_{12}^{(m)}), \tag{7b}$$
$$\Omega_{12}^{(c)}=\frac{K_1}{h_m}(1+\chi)S_{66}^{(m)},\quad a_1=-\frac{S_{12}^{(m)}+\chi S_{12}^{(c)}}{S_{11}^{(m)}+\chi S_{11}^{(c)}}$$

The in-plane layer stresses in the ceramic layer containing multiple transverse cracks can be used to evaluate the reduction of stiffness properties of the single domain sample due to multiple cracking. Instead of a cracked sample we consider a layered solid, in which the damaged layer is replaced with an equivalent homogeneous layer with degraded stiffness properties. The constitutive equations of the equivalent homogeneous layer are

$$\{\overline{\sigma}^{(c)}\}=[\overline{Q}^{(c)}]\{\overline{\varepsilon}^{(c)}\} \tag{8}$$

The in-plane macrostresses $\overline{\sigma}_{ij}^{(c)}$ and microstrains $\overline{\varepsilon}_{ij}^{(c)}$ in the equivalent homogeneous layer are determined as

$$\overline{\sigma}_{ij}^{(c)}=\frac{1}{2s}\int_{-s}^{s}\widetilde{\sigma}_{ij}^{(c)}dx_2,\quad \overline{\varepsilon}_{ij}^{(c)}=\overline{\varepsilon}_{ij}^{(m)}=\overline{\varepsilon}_{ij}=\frac{1}{2s}\int_{-s}^{s}\widetilde{\varepsilon}_{ij}^{(c)}dx_2 \tag{9}$$

The reduced in-plane stiffness matrix $[\overline{Q}^{(c)}]$ of the equivalent homogeneous layer is related to the in-plane stiffness matrix $[\hat{Q}^{(c)}]$ of the undamaged ceramic layer via the In-situ Damage Effective Functions (IDEFs) $\Lambda_{22}^{(c)}$, $\Lambda_{66}^{(c)}$, as

$$[\overline{Q}^{(c)}]=[\hat{Q}^{(c)}]-\begin{bmatrix}\dfrac{(\hat{Q}_{12}^{(c)})^2}{\hat{Q}_{22}^{(c)}}\Lambda_{22}^{(c)} & \hat{Q}_{12}^{(c)}\Lambda_{22}^{(c)} & 0\\ \hat{Q}_{12}^{(c)}\Lambda_{22}^{(c)} & \hat{Q}_{22}^{(c)}\Lambda_{22}^{(c)} & 0\\ 0 & 0 & \hat{Q}_{66}^{(2)}\Lambda_{66}^{(c)}\end{bmatrix} \tag{10}$$

The IDEFs $\Lambda_{22}^{(c)}$, $\Lambda_{66}^{(c)}$ can be expressed in terms of macrostresses $\overline{\sigma}_{ij}^{(c)}$ and macrostrains $\overline{\varepsilon}_{ij}^{(c)}$ as

$$\Lambda_{22}^{(c)}=1-\frac{\overline{\sigma}_{22}^{(c)}}{\hat{Q}_{12}^{(c)}\overline{\varepsilon}_{11}^{(c)}+\hat{Q}_{22}^{(c)}\overline{\varepsilon}_{22}^{(c)}}=1-\frac{1-\dfrac{D}{\lambda_1^{(c)}}\tanh\left[\dfrac{\lambda_1^{(c)}(1-D_w)}{D}\right]}{\dfrac{1+\lambda_1^{(c)}D_w}{1-D_w}+\alpha_1^{(c)}\dfrac{D}{\lambda_1^{(c)}}\tanh\left[\dfrac{\lambda_1^{(c)}(1-D_w)}{D}\right]} \tag{11a}$$

$$\Lambda_{66}^{(c)}=1-\frac{\overline{\sigma}_{12}^{(c)}}{\hat{Q}_{66}^{(c)}\overline{\varepsilon}_{12}^{(c)}}=1-\frac{1-\dfrac{D}{\lambda_2^{(c)}}\tanh\left[\dfrac{\lambda_2^{(c)}(1-D_w)}{D}\right]}{\dfrac{1+\lambda_2^{(c)}D_w}{1-D_w}+\alpha_2^{(c)}\dfrac{D}{\lambda_2^{(c)}}\tanh\left[\dfrac{\lambda_2^{(c)}(1-D_w)}{D}\right]} \tag{11b}$$

Here $D=\frac{h_c}{s}$ is the relative crack density, $D_w=\frac{l}{s}$ is the relative crack widening. Constants $\lambda_i^{(c)}=h_c\sqrt{L_i^{(c)}}$ and $\alpha_i^{(c)}, i=1,2$, depend solely on the compliances $\hat{S}_{ij}^{(m)}, \hat{S}_{ij}^{(c)}$ of metal and ceramic layer respectively, the shear lag parameters K_j and the layer thickness ratio χ, whereas

$$\alpha_1^{(c)}=\frac{1}{\chi}[\hat{Q}_{22}^{(c)}(\hat{S}_{22}^{(m)}+a_1\hat{S}_{12}^{(m)})+\hat{Q}_{12}^{(c)}(\hat{S}_{12}^{(m)}+a_1\hat{S}_{11}^{(m)})],\quad \alpha_2^{(c)}=\frac{1}{\chi}\hat{Q}_{66}^{(c)}\hat{S}_{66}^{(m)} \tag{12}$$

In order to verify the results of the analytical modelling and also to estimate numerically the thickness of the shear layer h_s introduced in the analytical model, finite element (FE) modelling of the composite sample in ABAQUS (ABAQUS, 2015) was also carried out. FE model corresponding to the layered metal/ceramic microstructure was created (Fig. 3). One quarter of the representative segment (Figure 2 b, c) was built in ABAQUS in order to investigate dependence of the stress field on the transverse co-ordinate x_3 for different crack spacings (parameter s). Parameter l like in the analytical model corresponds to crack widening. Boundary conditions reproducing tensile loading ($\overline{\sigma}_{11}=\overline{\sigma}_{12}=0$) were applied to the segment. Material behaviour of the metallic and ceramic layers was modelled as elastic. FE modeling allowed us to estimate numerically the thickness of the shear layer for different crack spacings and use these results in the analytical modelling.

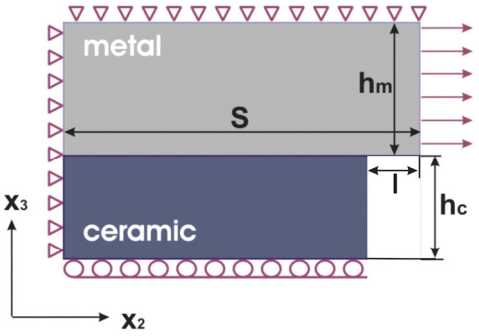

Fig. 3. FE model of a quarter of the representative segment with thicknesses $2h_c$ and h_m of the ceramic and metallic layers; $2s$ is the crack spacing und $2l$ is the crack widening.

3. Results and discussion

The following material properties were used in the calculations: Young's moduli of metal and ceramics are taken as 80 GPa and 390 GPa respectively; Poisson's ratios are 0.33 and 0.24 respectively, layer thicknesses are $h_m=0.3$ mm and $h_c=0.2$ mm, respectively.

Figure 4 shows normalized axial stress $\tilde{\sigma}_{22}^{(c)}/\overline{\sigma}_{22}$ as a function of distance x_2 for a range of half-spacing to layer thickness ratios s/h_c under uniaxial tensile loading ($\overline{\sigma}_{11}=\overline{\sigma}_{12}=0$). The shear layer thickness is taken as $h_s=0.15h_m$. According to the analytical model, the average axial stress between the two existing cracks is tensile, with its value decreasing as the distance between two neighboring cracks becomes smaller. At lower crack densities (i.e. larger crack spacing), the curve exhibits a characteristic plateau. Comparison of predictions with (Figure 4b) and without (Figure 4a) crack widening shows that for large crack spacings crack widening has little effect on the distribution of the axial stress. For small crack spacing, crack widening contributes to reduction of the maximum axial stress value at mid-point between the cracks.

To investigate stress field in the cracked composite in more detail, numerical modelling of metal/ceramic sample was carried out in ABAQUS using the model given in Figure 3. Distribution of axial stress $\sigma_{22}^{(c)}$ for three different crack spacings in the absence of crack widening ($D_w=0$) is shown in Figure 5. As can be seen in Figure 5a, for large crack spacings axial stress $\sigma_{22}^{(c)}$ in the ceramic layer between the cracks is tensile away from crack surfaces, however there is a region of compressive stress in the ceramic layer in the vicinity of the crack surface. As crack spacing becomes smaller, the compression region increases in size (Figure 5b, c). This is accompanied by high

tensile stresses in the ceramic layer in the vicinity of ceramic/metal interface, indicating the possibility of debonding as a competing failure mechanism.

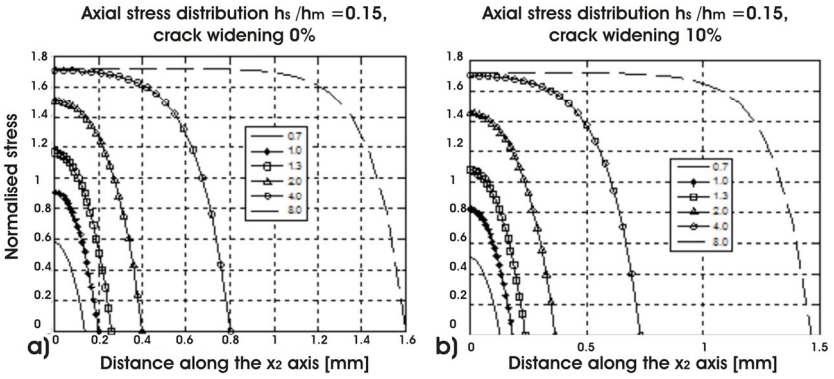

Fig. 4. Normalized axial stress $\widetilde{\sigma}_{22}^{(c)} / \overline{\sigma}_{22}$ in the ceramic layer as a function of co-ordinate x_2 for a range of crack spacing to layer thickness ratios as predicted by the analytical model: (a) no widening $D_w = 0.$; (b) with relative crack widening $D_w = 10\%$.

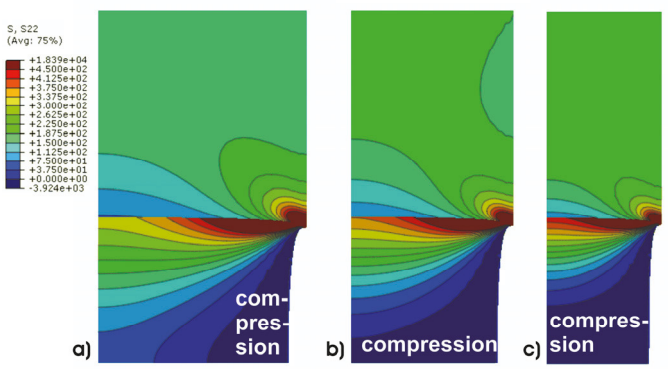

Fig. 5. Axial stress distribution in the cracked ceramic layer for three crack half-spacing to layer thickness ratios: (a) $s/h_c = 1.3$; (b) $s/h_c = 1.0$; (c) $s/h_c = 0.7$. No crack widening.

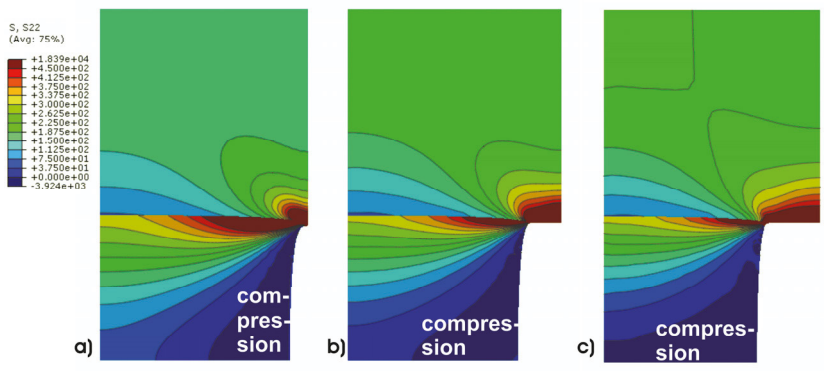

Fig. 6. Axial stress distribution in the cracked ceramic layer for $s/h_c = 1.3$: (a) without crack widening $D_w = 0.$; (b) with relative crack widening $D_w = 10\%$; c) with relative crack widening $D_w = 15\%$.

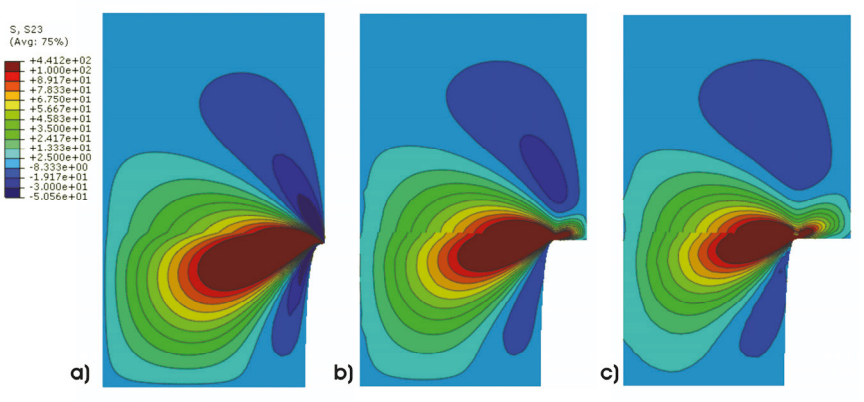

Fig. 7. Shear stress distribution in the cracked ceramic layer for three crack half-spacing to layer thickness ratio $s/h_c = 1.3$: a) without crack widening $D_w = 0.$; b) with relative crack widening $D_w = 10\%$; c) with relative crack widening $D_w = 15\%$.

Table 1.

	Normalised material property					
	Young's modulus E_2		Shear modulus G_{12}		Poisson's ratio ν_{21}	
Relative crack density D	$D_w = 0.$	$D_w = 10\%$	$D_w = 0.$	$D_w = 10\%$	$D_w = 0.$	$D_w = 10\%$
0.2	0.6461	0.5755	0.8566	0.6927	0.6779	0.6136
0.4	0.4903	0.4470	0.7404	0.6075	0.5361	0.4967
0.6	0.4059	0.3767	0.6446	0.5355	0.4593	0.4593
0.8	0.3571	0.3365	0.5657	0.4754	0.4149	0.4327
1.0	0.3276	0.3126	0.5018	0.4269	0.3881	0.3744

Figure 6 shows the axial stress distribution for crack half-spacing to thickness ratio $s/h_c = 1.3$ with and without crack widening. For the crack without widening (Figure 6a), stress $\sigma_{22}^{(c)}$ in the ceramic layer is tensile between the cracks away from crack surfaces, however there is a region of compressive stress in the ceramic layer in the vicinity of the crack surface. For the crack with 10% relative crack widening the compression region is larger; for 15% relative crack widening, stress $\sigma_{22}^{(c)}$ is compressive in the entire region between the cracks and development of the new crack in between is not possible. The same figure shows also other effect of the crack widening: the $\sigma_{22}^{(c)}$ stress in the interface region between metal and ceramic decreases and large region of higher $\sigma_{22}^{(c)}$ stress progressively increases above the widening. For the crack with widening, only one possible development of the damage is to progress into the metal layer which in turn will lead to an increase of the crack widening.

Crack widening also changes the distribution of shear stresses in the vicinity of the crack tip and the crack tip region. Figure 7 shows shear stress distribution for $s/h_c = 1.3$. It is evident that the region with higher shear stress decreases with increasing of the crack widening and it creates the new zone of higher stresses near the corner (see Figure 7c).

The effect of cracks in the ceramic layers on the overall stiffness of the metal/ceramic composite sample has been also investigated. Table 1 shows stiffness properties of the composite sample normalized by their values in the undamaged state, as predicted by the analytical model for a range of relative crack densities $D = \frac{h_c}{s}$. Crack-induced changes are predicted for Young's modulus E_2, Shear modulus G_{12} and Poisson's ratio ν_{21}. Comparison of predictions with relative crack widening ($D_w = 10\%$) and without crack widening ($D_w = 0.$) shows that cracks with widening produce greater reduction in the composite's stiffness. Experimental data are required to validate these predictions, which are currently not available in the literature and this could become a task of future work.

Conclusions

The influence of crack distances and crack widening on the stress distribution in metal-ceramic composites with lamellar microstructure was studied using analytical and FE methods. FE model predicted the development of the compressive zone in between the cracks for small distances between the cracks. Crack widening accelerates this process. The presence of crack widening also influences the $\sigma_{22}^{(c)}$ stress distribution: the highest stresses are in the top of the widening and the stresses on the metal-ceramic interface decrease with increasing of the widening. Obtained results predict damage process in the metal phase (plastic flow) which in turn will lead to larger widening of the crack. Using the analytical model, the effect of cracks in the ceramic layer on the overall stiffness of the metal-ceramic composite has been estimated. Predictions show that Young's modulus E_2 in the direction normal to the cracks, Shear modulus G_{12} and Poisson's ratio ν_{21} are significantly reduced when the cracks are present. Crack widening contributes to further reduction of these stiffness properties. Present studies were motivated by the available experimental results, mostly in the form of images of the progressive failure of the single domain samples under compressive loading. Performing tensile tests on the single domains will provide the necessary verification of the predicted damage process including cracking development, crack spacing and development of the widening.

Acknowledgements

The financial support of The Royal Society (UK) International Exchanges grant IE121116 and DFG (PI 785/1-2, PI 785/3-2) and Darmstadt University of Applied Sciences is gratefully acknowledged. We thank Dr. K. G. Schell, Prof. M. J. Hoffmann and Dr. R. Oberacker of the ceramics lab of the Institute for Applied Materials at Karlsruhe Institute of Technology for providing the alumina preforms and Dr. S. Roy for helpful discussions about damage process in MMCs.

References

ABAQUS, Simulia, Providence, RI, USA, http://www.3ds.com/products-services/simulia/, Accessed 4 June 2015.

Deville, S., 2008. Freeze-Casting of Porous Ceramics: A Review of Current Achievements and Issues, Advanced Engineering Materials, 10(3), 155-169.

Kashtalyan, M., Sinchuk, Y., Piat, R., Guz, I., 2016. Analysis of multiple cracking in metal/ceramic composites with lamellar microstructure, Arch Appl Mech 86(1), 177-188.

Kashtalyan, M., Soutis, C., 2013. Predicting residual stiffness of cracked composite laminates subjected to multi-axial inplane loading. Journal of Composite Materials 47 (20-21), 2513-2524

Kashtalyan, M,, Soutis, S., 2011. Residual stiffness of cracked cross-ply composite laminates under multi-axial in-plane loading. Applied Composite Materials 18: 31-43.

Mortensen, A., Llorca, J., 2010. Metal Matrix Composites. Annual Review of Materials Research 40: 243-270.

Roy, S., Butz, B., Wanner, A., 2010. Damage evolution and domain-level anisotropy in metal/ceramic composites exhibiting lamellar microstructures, Acta Materialia 58, 2300–2312.

Roy, S., Gebert, M.-J., Stasiuk, G., Piat, R., Weidenmann, K.A., Wanner, A., 2011. Complete determination of elastic moduli of interpenetrating metal/ceramic composites using ultrasonic techniques and micromechanical modeling, Materials Science and Engineering A, 528 (28), 8226-8235.

Roy, S., A. Wanner, A., 2008. Metal/ceramic composites from freeze-cast ceramic preforms: Domain structure and elastic properties, Composite Science and Technology, 68, 1136–1143.

Sinchuk, Y., Roy, S., Gibmeier, J., Piat, R., Wanner, A., 2013. Numerical study of internal load transfer in metal/ceramic composites based on freeze-cast ceramic preforms and experimental validation, Materials Science & Engineering A, 585, 10–16.

Ziegler, T., Neubrand, A., Roy, S., Wanner, A., Piat, R., 2009. Elastic constants of metal/ceramic composites with lamellar microstructures: Finite element modelling and ultrasonic studies, Composite Science and Technology, 69 (5), 620-626.

Ziegler, T., Neubrand, A., Piat, R., 2010. Multiscale homogenization models for the elastic behaviour of metal/ceramic composites with lamellar domains, Composites Science and Technology, 70(4), 664–670.